Two *b*'s or not two *b*'s

F. Alejandro Nava Pichardo[1], Víctor Hugo Márquez-Ramírez[2,*], F. Rámon Zúñiga Dávila-Madrid[2], Lenin Ávila-Barrientos[1,3]

[1] Centro de Investigación Científica y de Educación Superior de Ensenada, Baja California. División de Ciencias de la Tierra, Departamento de Sismología. Carretera Ensenada – Tijuana No. 3918, Zona Playitas, 22860, Ensenada, Baja California, México.

[2] Universidad Nacional Autónoma de México, Instituto de Geociencias, Blvd. Juriquilla No. 3001, Querétaro, 76230, México.

[3] Dirección Adjunta de Investigación Humanística y Científica, SECIHTI, Av. Insurgentes Sur 1582, Col. Crédito Constructor, Alcaldía Benito Juárez, C. P. 03940, Ciudad de México.

*Corresponding author: marvh@geociencias.unam.mx

F. Alejandro Nava Pichardo

https://orcid.org/0000-0001-6778-2017

Víctor Hugo Márquez-Ramírez

https://orcid.org/0000-0003-1494-2229

F. Rámon Zúñiga Dávila-Madrid

https://orcid.org/0000-0003-0277-3034

Lenin Ávila-Barrientos

https://orcid.org/0000-0001-7451-8636

Abstract

The b-value, a crucial parameter in the Gutenberg-Richter magnitude distribution, plays a pivotal role in understanding seismic activity. Its significance stems primarily from its inverse correlation with stress levels in the Earth's crust, offering valuable insights into the underlying forces that drive earthquake occurrences. The case when a data sample contains events from two different populations having different b-values is considered, and how the G-R histogram will feature a change in slope that tends asymptotically to the smallest of the b-values is demonstrated. It is shown how, given enough data, the parameters of the two populations can be approximately recovered, and provide both numerical examples and applications to real data.

Key words: Gutenberg-Richter b-value; Composite statistical populations; Recovering different b-values; Statistical seismology

1 Introduction

A most important statistical tool widely used in seismological studies is the Gutenberg-Richter magnitude distribution (Ishimoto and Ida,1939; Gutenberg and Richter,1944; Richter, 1958)

$$\log_{10} N(M) = a - b\,(M - M_c); \quad M \geq M_c \tag{1}$$

where $N(M)$ is the number of magnitudes $\geq M$, $a = \log_{10} N(M_c)$ is the total number of sample data, b describes the proportion of large magnitudes to small ones (Richter, 1958), and M_c is the completeness magnitude below which $\log_{10} N(M)$ ceases to behave linearly due to insufficient seismographic coverage (e.g., Wiemer and Wyss, 2002).

The b parameter is quite important for several reasons; not only does it help to estimate occurrence rates for different magnitudes (within limits that will be mentioned below), but it gives information about physical characteristics of the seismicity. Since the G-R distribution implies a power-law relationship for the seismic moment, b gives information about the scaling of the seismic sources (e.g., Rundle, 1989; Okal and Kirby, 1995; Main et al, 2000; Fujii and Matsumura, 2001; Rundle et al., 2003; Madariaga, 2010; Amitrano, 2012). Further information about the spatial distribution of sources is the proposed relationship between *b* and fractal dimension (e.g., Aki, 1981; Hirata, 1989; Oncel et al., 2001; Wyss et al., 2004; Singh et al. 2009), and *b* and magnitude entropy (Mansinha and Shen, 1987; Main and Al-Kindy, 2002; Nava, 2024).

Probably, the most important feature of *b* is its inverse relationship with the stress level (Wyss, 1973; Frohlich and Davis, 1993; Enescu and Ito, 2001; Utsu, 2002; Wyss et al., 2004; Nuannin et al., 2005; Schorlemmer et al, 2005; Nanjo et al., 2012; El-Isa and Eaton, 2014; Scholtz, 2015; Wang, 2016; DeSalvio and Rudolph, 2021; Li and Chen, 2021; Godano et al., 2024; Hu et al, 2024; and many others), which gives *b* a most important role in earthquake hazard estimation and forecasting.

The G-R distribution does not contemplate an upper limit for *M*, but there are physical limits to how large a magnitude can be (e.g., Olsson, 1999; Kijko, 2004), and it has been proposed that the G-R distribution should be truncated or otherwise modified for extremely large magnitudes (e.g., Sornette et al., 1996; Sornette and Sornette, 1999; Burroughs and Tebbens, 2002). Below the megaquake level, discontinuities in the slope of the G-R distribution have been observed, and the changes to higher values of *b* occurring for $M \sim 7.5$ have been explained in terms of changes in source scaling due to characteristic sizes of the seismogenic regions (Scholz, 1982; Singh et al., 1983; Pacheco et al, 1992; Romanowicz and Rundle, 1993; Scholz, 1997; Main et al., 1999; Amitrano, 2003; Pisarenko and Sornette, 2004).

Sometimes G-R histograms feature another change in slope for magnitudes smaller than the above mentioned ones; some examples are: Singh et al. (1983), Okal and Kirby (1995), Triep and Sykes (1997), Wiemer and McNutt (1997), Wyss et al. (1997), Wiemer and Wyss (2002), Amorese (2007), Zhan (2017). A sharp change in slope occurring always at the same magnitude can be explained by different magnitude scales being used for two different magnitude ranges (e.g., Ávila-Barrientos and Nava, 2020), while gradual increases in slope can be caused by insufficient sampling.

In the present work, the possibility that a sample be taken from two different populations with different *b*-values will be considered, to see what changes such a mixture can cause in the G-R histogram, and a method to recover these values approximately will be proposed. At first, the theoretical case is presented, then the results are justified through numerical simulation, which shows which ranges of b-values are identifiable under which sample sizes. Finally, two examples of application to real data from different tectonic regimes are presented.

2 *b*-value estimation

For the distribution (1) b-values can be estimated directly from the slope of the linear range on the G-R histogram (e.g. Guttorp, 1987), but frequently b-values are estimated from the mean magnitude (Aki, 1965; Utsu, 1965; Tinti and Mulargia, 1987; Marzocchi and Sandri, 2003), using the Aki-Utsu maximum likelihood estimate

$$b = \frac{\log_{10}(\mathrm{e})}{\bar{M} - m_c}, \tag{2}$$

where $\bar{M}$ is the observed mean of the data and $m_c = M_c - \Delta M/2$, ΔM is the rounding interval, and M_c is the rounded magnitude of completeness. (Aki, 1965; Utsu, 1965).

The G-R distribution (1) is a reverse cumulative histogram corresponding to an exponential magnitude probability density function,

$$p(m) = \beta\ \mathrm{e}^{-\beta\,(m-m_c)};\ \ m \geq m_c \tag{3}$$

where

$$\beta = b\ \ln(10) = 1/\left(\mu - m_c\right), \tag{4}$$

and μ is the mean of the exponential distribution.

3 Two *b*s

Suppose there is a region of interest where seismicity corresponds to two different populations with different b-values. This could be the case, for instance, when a largish earthquake has occurred within the region, but it was not large enough to liberate all stresses in the region, and it is not practical to try to discriminate between areas having different stresses. Another instance would be when volcanic or geothermal activity associated with high b-values is present within a seismogenic region.

In such a region the population is a composite of two GR-distributed populations, one consisting of N_1 elements distributed exponentially with parameter β_1, and another with N_2 elements and parameter β_2. The total number of observed events, $N_T = N_1 + N_2$, will be distributed as

$$n(M) = N_1\beta_1 \mathrm{e}^{-\beta_1(M-M_c)} + N_2\beta_2 \mathrm{e}^{-\beta_2(M-M_c)} , \tag{5}$$

and the corresponding pdf is

$$f(M) = \frac{N_1}{N_T}\beta_1 \mathrm{e}^{-\beta_1(M-M_c)} + \frac{N_2}{N_T}\beta_2 \mathrm{e}^{-\beta_2(M-M_c)} , \tag{6}$$

with mean

From $\quad \int x\mathrm{e}^{cx}\mathrm{d}x = \mathrm{e}^{cx}\left(\frac{cx-1}{c^2}\right)$

$$\int_{M_c}^{\infty} M\beta_1 \mathrm{e}^{-\beta_1(M-M_c)}\mathrm{d}M = \beta_1 \mathrm{e}^{\beta_1 M_c} \int_{M_c}^{\infty} M\mathrm{e}^{-\beta_1 M}\mathrm{d}M = \frac{1}{\beta_1} + M_c$$

$$\bar{M} = \mathrm{E}[f(M)] = \frac{N_1}{N_T}\left(\frac{1}{\beta_1} + M_c\right) + \frac{N_2}{N_T}\left(\frac{1}{\beta_2} + M_c\right) , \tag{7}$$

From (4) and (7),

$$\bar{M} = \frac{N_1}{N_T}\bar{M}_1 + \frac{N_2}{N_T}\bar{M}_2 , \tag{8}$$

so the observed $\bar{M}$ will have a value intermediate between $\bar{M}_1$ and $\bar{M}_2$. Hence, the b-value estimated from the Aki-Utsu relation (2), b_m, will have a value intermediate between b_1 and b_2,

$$\frac{1}{b_m} = \frac{N_1}{N_T}\frac{1}{b_1} + \frac{N_2}{N_T}\frac{1}{b_2} \tag{9}$$

Figure 1 shows an example of how b_m varies with the fraction $\frac{N_1}{N_T}$ for given $b_1 = 0.8$ and $b_2 = 1.2$; note that for $N_1 = N_2$ the observed $b_m = 0.960 \neq (b_1 + b_2)/2$.

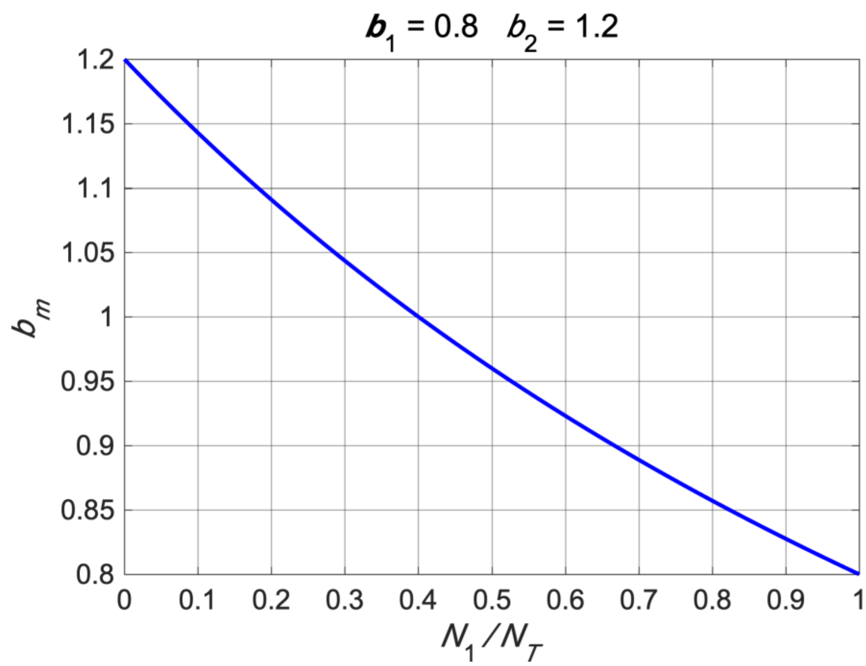

Fig. 1 Measured b_m value for $b_1 = 0.8$ and $b_2 = 1.2$ for different relative values of N_1/N_T.

Knowing only N_T and b_m, can the parameters of the original populations be recovered? In principle, yes, if recourse to the G-R histogram of the observed data is taken; as explained below.

The measured G-R distribution is the logarithm of the reverse cumulative of the pdf, thus from (6)

$$F(M) = \int_{M_c}^{M} f(m)\,\mathrm{d}m = \frac{N_1}{N_T}\left(1 - \mathrm{e}^{-\beta_1(M-M_c)}\right) + \frac{N_2}{N_T}\left(1 - \mathrm{e}^{-\beta_2(M-M_c)}\right) \qquad (10)$$

and

$$F_{GR}(M) = 1 - F(M) = 1 - \frac{N_1}{N_T} - \frac{N_2}{N_T} + \frac{N_1}{N_T}\mathrm{e}^{-\beta_1(M-M_c)} + \frac{N_2}{N_T}\mathrm{e}^{-\beta_2(M-M_c)}$$

$$F_{GR}(M) = \frac{N_1}{N_T} \mathrm{e}^{-\beta_1(M-M_c)} + \frac{N_2}{N_T} \mathrm{e}^{-\beta_2(M-M_c)}$$

so that

$$N(M) = N_T F_{GR}(M) = N_1 \mathrm{e}^{-\beta_1(M-M_c)} + N_2 \mathrm{e}^{-\beta_2(M-M_c)} \, . \tag{11}$$

which is the G-R distribution resulting from the mixing of two samples from different populations.

Choosing $\beta_1 < \beta_2$, let (11) be written as

$$N(M) = N_1 \mathrm{e}^{-\beta_1(M-M_c)} \left[1 + \frac{N_2}{N_1} \mathrm{e}^{-(\beta_2-\beta_1)(M-M_c)}\right],$$

and taking logarithms

$$\log_{10} N(M) = a_1 - b_1(M - M_c) + \log_{10} \left[1 + \frac{N_2}{N_1} \mathrm{e}^{-(\beta_2-\beta_1)(M-M_c)}\right],$$

where $a_1 = \log_{10} N_1$, and may be written as

$$\log_{10} N(M) = a_1 - b_1(M - M_c) + \Gamma \, , \tag{12}$$

where

$$\Gamma \equiv \log_{10} \left[1 + \frac{N_2}{N_1} \mathrm{e}^{-(\beta_2-\beta_1)(M-M_c)}\right] . \tag{13}$$

Equation (12) tells that the observed G-R histogram for the combined populations, called henceforward GR, can be seen as the G-R histogram of the b_1 population, $a_1 - b_1(M - M_c)$, which will be called GR_1, plus the Γ term.

Figure 2 shows GR, GR_1, and the G-R histogram of the b_2 population, $a_2 - b_2(M - M_c)$, where $a_2 = \log_{10} N_2$, which will be called GR_2. It also shows the Γ term and the straight line $a_m - b_m(M - M_c)$, which will be referred to as GR_m, where $a_m = \log_{10} N_T$ and b_m is the slope estimated from the mean magnitude (8).

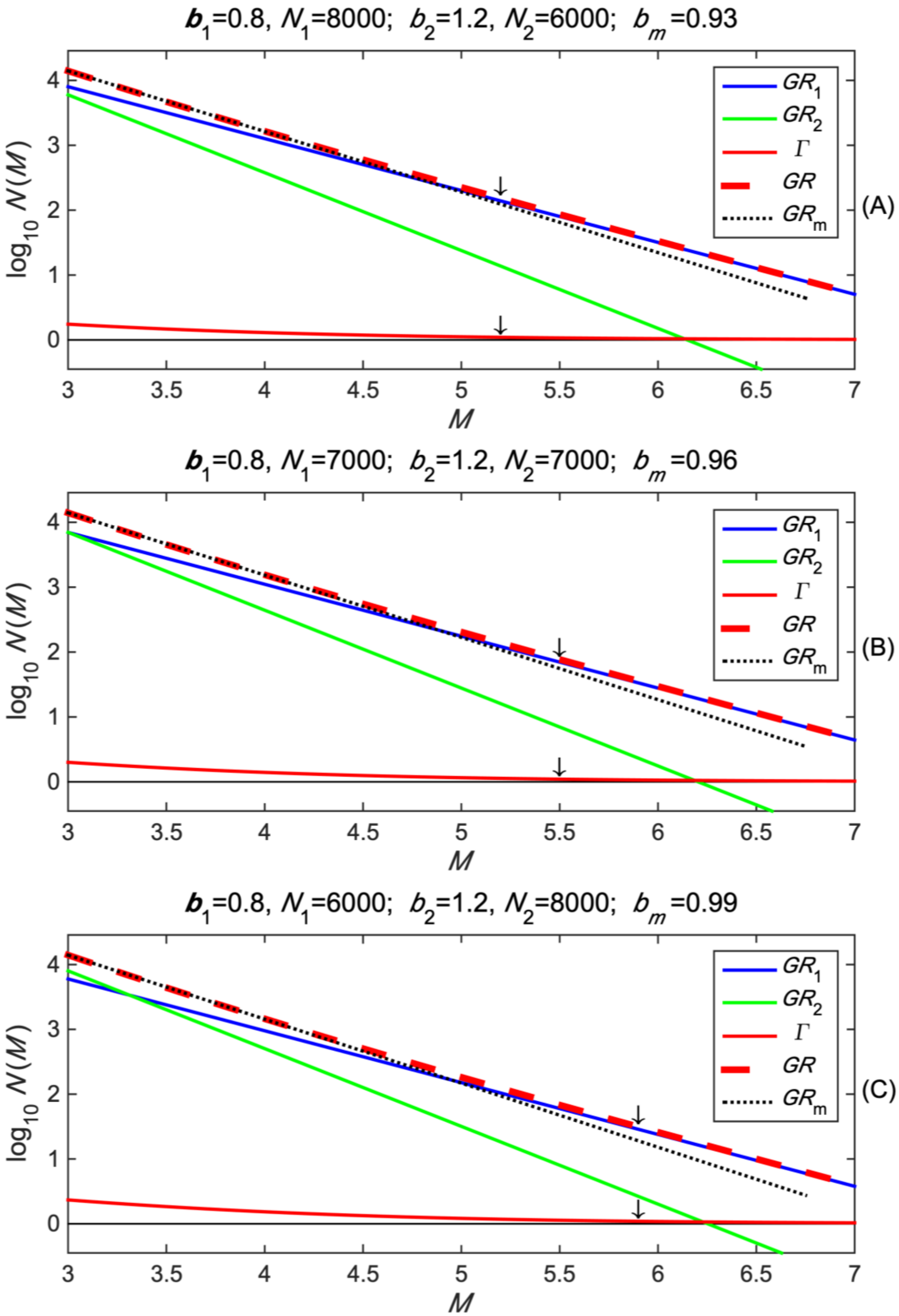

Fig. 2 Magnitude G-R distributions for data from two populations with $b_1 = 0.8$ and $b_2 =$

1.2 for different number of events corresponding to each population. The blue and green lines indicate the distributions for b_1 and b_2, respectively; the thick red line is the G-R distribution for the combined data, and the dotted black line shows the distribution inferred from the measured b_m; the black line shows the Γ function (13). Panels (A), (B), and (C) show results for $N_1 > N_2$, $N_1 = N_2$, and $N_1 < N_2$, respectively. Arrows above the Γ and GR histograms indicate the magnitudes for which Γ, is smaller than $\log_{10} N_T$ by a factor of 0.01.

4 Recovery of the individual distributions

The observed GR graph is not a straight line; for small magnitudes it is well fitted by GR_m, but differs from it as its slope diminishes for higher magnitudes, as will be discussed below. Here is a caveat for b estimations based on small samples that do not show clearly the change in slope, which is not seen or is attributed to a random superavit of large magnitudes.

As shown in Figure 2, the Γ term is maximum for $M = M_c$, where its value depends on the ratio N_2/N_1. Now, if $N_1{\sim}N_2$ is assumed, because if one of the populations is much smaller than the other then its contribution to (5) will not be significant and can be ignored, then the ratio will be in the ~0.5 to ~2.0 range, and a Γ maximum in the ~0.176 to ~0.477 range can be expected. The Γ term diminishes as magnitudes increase at a ratio that depends on $\Delta\beta = \beta_2 - \beta_1$. Thus, the GR histogram tends asymptotically to GR_1 for large magnitudes, and although Γ will not be strictly zero within the practical magnitude range, it can attain values much smaller than $\log_{10} N_T$. Arrows above the Γ and GR histograms indicate the magnitude for which $\Gamma \leq \gamma \log_{10} N_T = \log_{10} N_T^{\gamma}$, for a factor $\gamma = 0.01$, and it can be seen that, from that magnitude on, Γ decreases quite slowly and becomes approximately parallel to GR_1, so that a fit of a straight line to the tail of the distribution can estimate both b_1 and, approximately, N_1.

Figure 3 shows how M_γ, the magnitude at which $\Gamma = \gamma \log_{10} N_T$, varies for different values of N_2/N_1 and $b_2 - b_1$ for $\gamma = 0.01$ and $N_T = 14{,}000$.

$$\Gamma \equiv \log_{10}\left[1 + \frac{N_2}{N_1} \mathrm{e}^{-(\beta_2-\beta_1)(M-M_c)}\right] = \gamma \log_{10} N_T$$

$$M_\gamma - M_c = -\ln\left[\frac{N_1}{N_2}\left(N_T^\gamma - 1\right)\right] / [(b_2 - b_1)\ln 10]$$

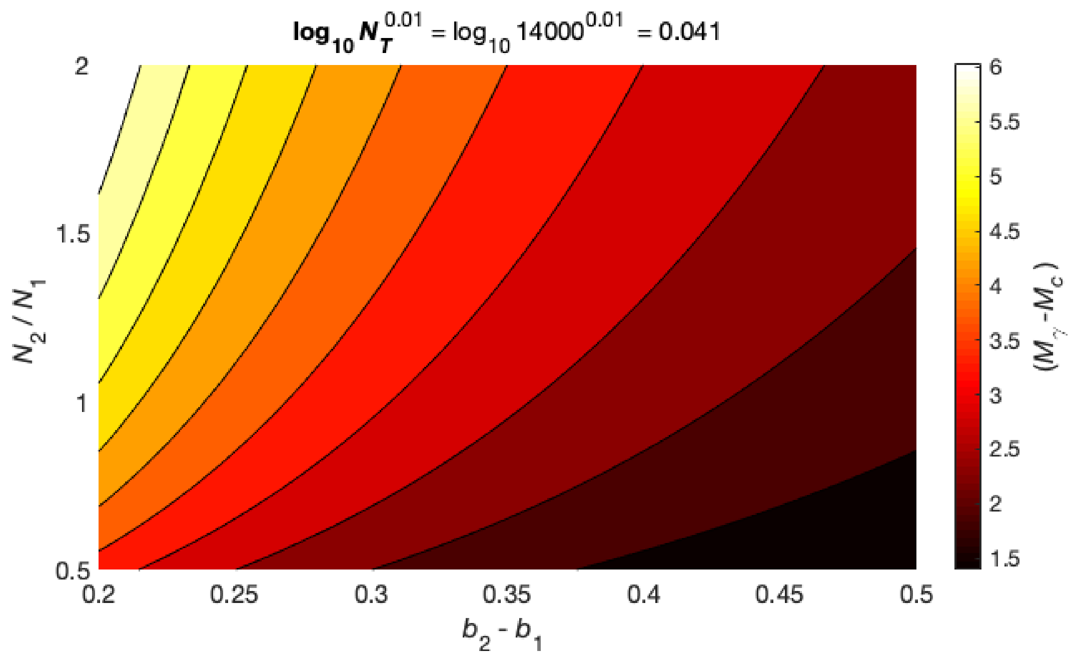

Fig. 3 Variation of M_γ for different values of N_2/N_1 and $b_2 - b_1$.

From N_1 and N_T,

$$N_2 = N_T - N_1 \tag{14}$$

can be easily estimated, so it only remains to estimate b_2.

From (4) and (8)

$$\left(\frac{\log_{10}\mathrm{e}}{b_m} + M_c\right) = \frac{N_1}{N_T}\left(\frac{\log_{10}\mathrm{e}}{b_1} + M_c\right) + \frac{N_2}{N_T}\left(\frac{\log_{10}\mathrm{e}}{b_2} + M_c\right)$$

so that

$$b_2 = N_2\left(\frac{N_T}{b_m} - \frac{N_1}{b_1}\right)^{-1}, \tag{15}$$

and all parameters have been approximately estimated.

5 Numerical example

Next, it will be shown whether synthetic sets consisting of exponentially distributed magnitudes randomly generated for two exponential populations with different *b*-values and different sizes do distribute according to (12) and exhibit the features seen in the analytic treatment. Simulations are useful because they can help to identify possible limitations and problems in treating with data, that do not appear for the analytic treatment.

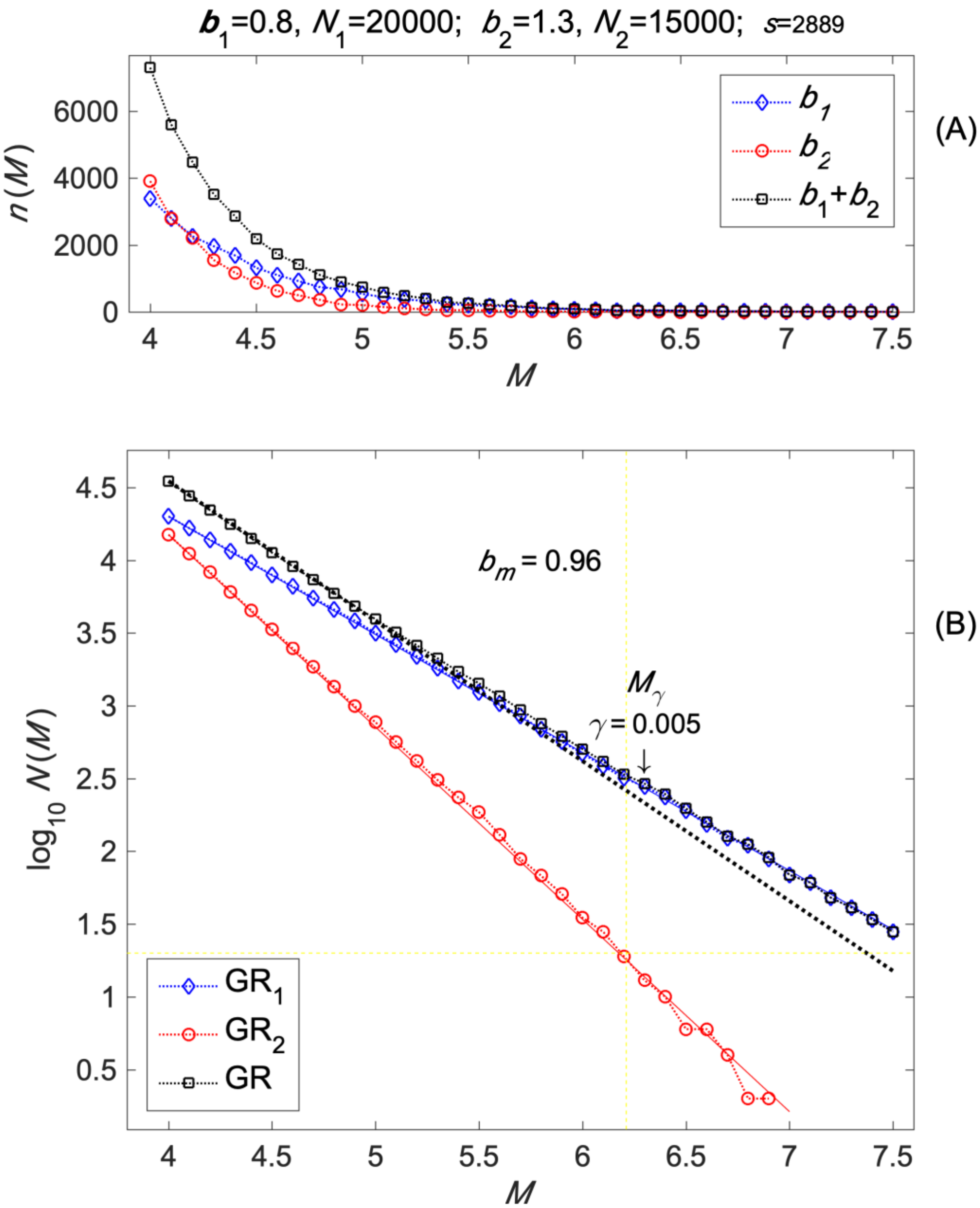

Fig. 4 Exponential distributions for two synthetic exponentially distributed populations with $b_1 = 0.8$, $b_2 = 1.3$, respectively, and their sum for $M_c = 4.0$ (A). The corresponding G-R distributions as identified in the legend and, in the same color, the straight lines for each of the populations (B), showing the measured b_m and an arrow indicating the magnitude corresponding to $\gamma = 0.005$.

Figure 4 shows an example of a synthetic realization; on top (A) are shown the exponential distributions for the two populations with different *b*-values and the distribution resulting from considering the two populations as one, and below (B) are shown the G-R histograms for each of the populations, GR_1 and GR_2, and for the combined population, GR, together with the straight lines for to the individual populations and for the Aki-Utsu analysis of the combined population.

The figure shows expected behavior and other plausible features. It also shows the effects of the main limitation of this and other statistical studies: i.e., scarcity of data for large magnitudes.

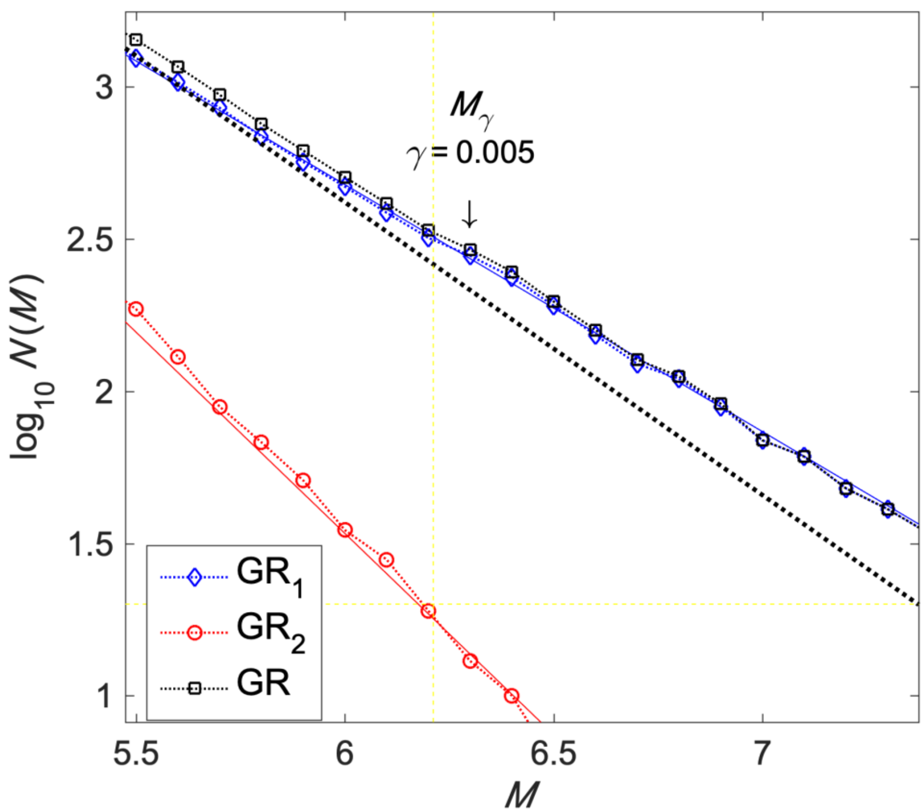

Fig. 5 Close-up of Figure 4.

Figure 5 again illustrates the major problem in recovering the distribution parameters: even though this example has an unrealistic large number of data, large magnitudes are not numerous enough for the histogram to approach the b_1 slope, so this parameter will be overestimated. The problem is, of course, worse for smaller samples.

The strategy to follow is to look for the magnitude range that, when fitted by least-squares, results in the smallest b_1 value. Results are not bad: in this example, it is possible to identify this parameter with an error of less than 6%.

This overestimate, however, also results in an overestimate of N_1 so that b2 from (15) is oversestimated and N2 from (16) is underestimated; however, the actual value of these parameters is not very important, because for precursory purposes it is important to detect the underlying low b values.

6 Application

As a first illustration of the application to real data, data from the RESNOM network for northern Baja California will be used. Figure 6 shows the study area, the epicenters for events $M \geq 2.5$ for 2012 to mid 2024, the main faults, the international Mexico/US border, and the location of the El Mayor-Cucapah (EMC) $M_W = 7.2$ earthquake of April 4, 2010.

Earthquakes occurring close to the rupture area of the EMC event can be expected to have a high b-value corresponding to a stress-depleted volume, but it is very hard to separate these earthquakes from the surrounding seismicity, hence the method presented above will be applied to the whole seismicity.

The analysis is shown in Figure 7, where the G-R line shows a discontinuity around $M = 4.3$ to 4.4 and an apparent $b_m = 0.990$, the change in slope occurs around magnitude 4.2, and the minimum slope, corresponding to $b_1 = 0.709$, is found for magnitudes between 4.4 and 4.7, and $b_2 = 1.207$ would correspond to the low-stress population.

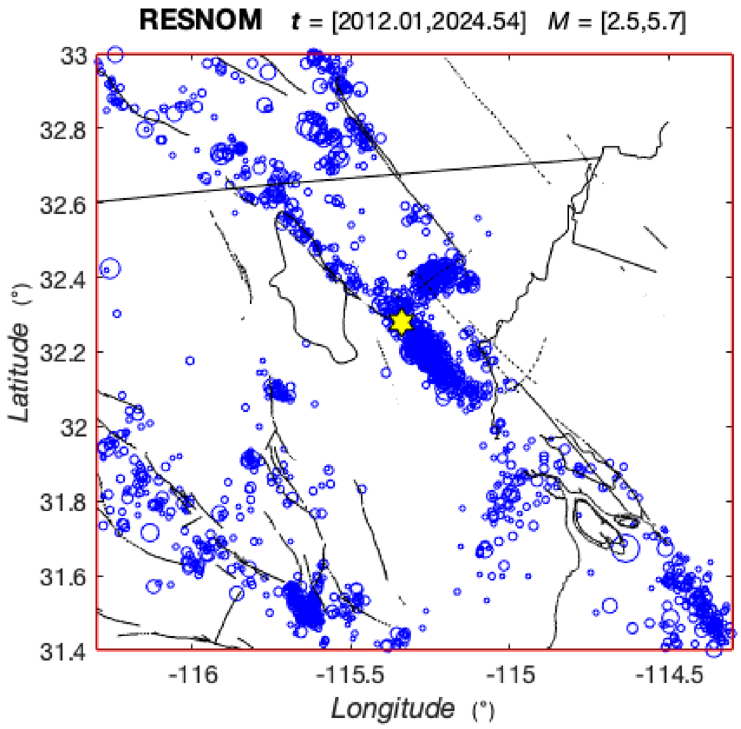

Fig. 6 Seismicity for the region around the EMC earthquake is indicated by the yellow hexagon; blue circles are epicenters, and thin lines indicate the principal local faults and the Gulf of California coastline. The thick, straight line is the international Mexico-USA border.

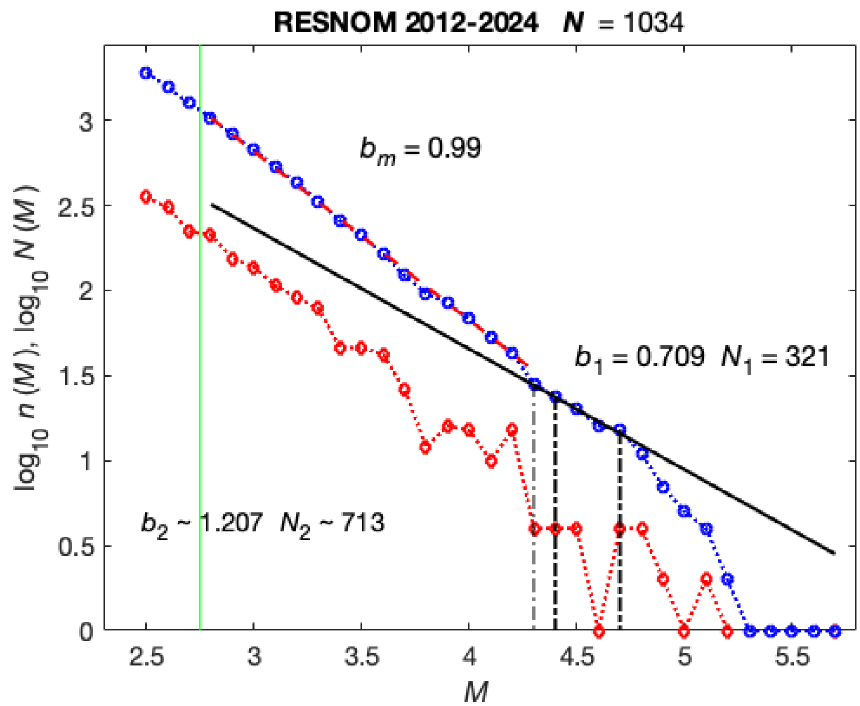

Fig. 7 G-R distribution corresponds to the seismicity of Fig. 6 (blue circles) and the non-cumulative distribution (red circles); the green line indicates M_c. The dashed line is the fit to the smaller magnitudes' distribution resulting in $b_m = 0.99$, and the thick black line is the fit to the b_1 slope.

As a second illustration, earthquakes in northern Chile (Fig.8) between August 1, 2000 and August 8, 2024 in a region that comprises the site of the September 2015 M_W 8.3 earthquake, and a region to the North where no large earthquakes have occurred recently will be considered. Data were downloaded from the USGS Search Earthquake Catalog https://earthquake.usgs.gov/earthquakes/search/

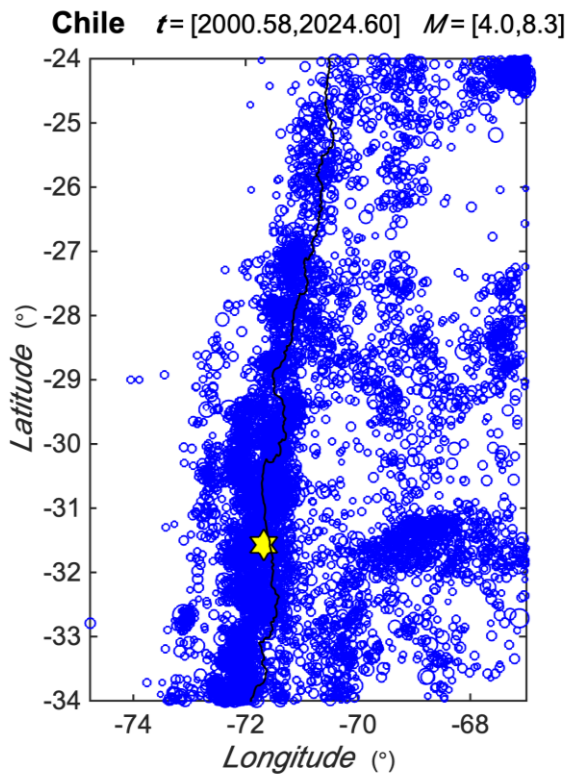

Fig. 8 Seismicity for the region around the 2015 M_W 8.3 earthquake is indicated by the yellow hexagon; blue circles are epicenters, and the black line indicates the Pacific Ocean coastline.

The corresponding analysis is shown in Figure 9, where the apparent $b_m = 1.17$, a change in slope can be seen around $M = 5.6$, which leads to $b_1 = 0.841$ and $b_2 = 1.719$.

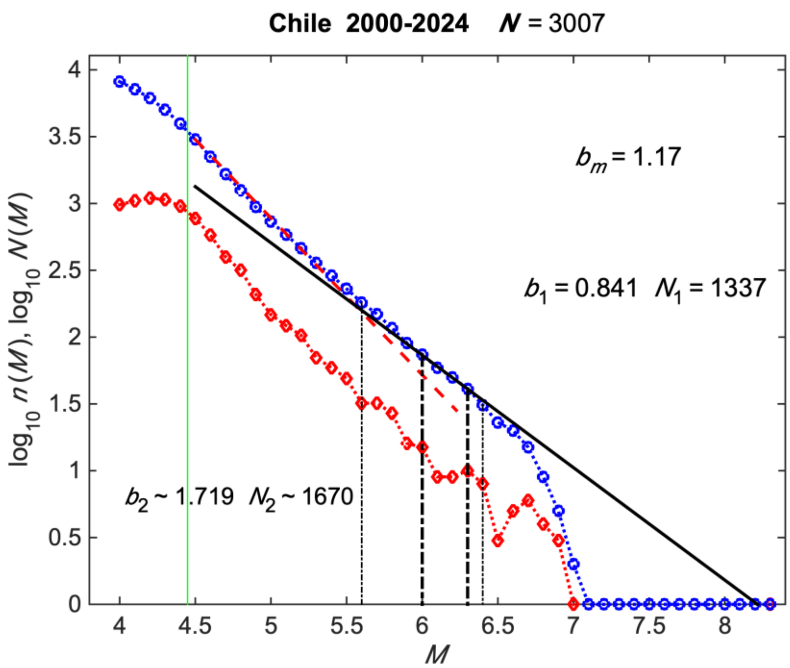

Fig. 9 G-R distribution corresponds to the seismicity of Fig. 8 (blue circles) and the non-cumulative distribution (red circles); the green line indicates M_c. The dashed line is the fit to the smaller magnitudes' distribution resulting in $b_m = 1.17$, and the thick black line is the fit to the b_1 slope.

Besides giving the important values of b_1 and b_2, the estimated values of N_1 and N_2 are also important, because dividing them by the total observation time yields the activity rates of both processes, which can be used to obtain estimates of Poissonian occurrence probabilities for given time intervals. The relative sizes of N_1 and N_2 clearly show which process is more active; the results from Figure 7 indicate that for the data from Baja California the process corresponding to b_1 is only about half (0.45) as active as that corresponding to b_2, while for Chile (Fig. 9) the ratio $N_1/N_2 = 0.80$ shows both processes to be approximately equally active.

7 Discussion and Conclusions

The case of catalog data being a mixture of two GR distributed populations with different b-values has been considered, and it has been shown that in some cases it may be possible to identify approximately the b-values and number of events in each population. This setup is not rare and may be due to aftershocks of large events being included in the data or including data from volcanic or geothermal sources together with data from tectonic earthquakes.

Whatever the b-values and the relative population sizes, as long as these are large enough, the observed change in slope is always from larger to smaller as magnitudes increase. Thus, changes in slope from smaller to larger must be due to some other mechanism like the one mentioned above for magnitudes ~7.5.

The main problem in the application is (as always for statistical studies) having enough data, because if any or both of the populations do not have enough events above the magnitude where b_1 could be identified, then the distribution will appear to be a standard distribution with one slope b_m. If this is the case, extrapolation of rates for large magnitudes will be underestimated (e. g., Singh et al., 1983).

If two slopes are identified, then there are two G-R distributions to base estimates of future activity on, but since the one for b_1 corresponds to the largest regional stress, it should be the one appropriate for the highest occurrence rate of large magnitudes, and hence the one to be used for hazard studies.

Acknowledgments

LA-B work was supported by SECIHTI *Investigadoras e Investigadores por México* program, project 7095.

Declarations

Competing Interests

The authors declare that there are no conflicts of interest or competing interests.

Authorship contribution statement

F.A.Nava: Conceptualization, programs, development, first draft. All authors: discussion, development, drafts. All authors discussed and approved the final manuscript.

Funding

This study had no external funding.

References

Aki, K. (1965) Maximum likelihood estimate of b in the formula log(N) = a - bM and its confidence limits, *Bull. Earthq. Res. Inst. Tokio Univ.* **43,** 237–239.

Aki, K. (1981) A probabilistic synthesis of precursory phenomena, in *Earthquake Prediction: An International Review*, Maurice Ewing Set., vol. 4, edited by D. W. Simpson and P. G. Richards, pp. 566-574, AGU, Washington, D.C. https://doi.org/10.1029/ME004p0566

Amitrano, D. (2003) Brittle-ductile transition and associated seismicity: Experimental and numerical studies and relationship with the b value, J. Geophys. Res., 108(B1), 2044, https://doi.org/10.1029/2001JB000680

Amitrano, D. (2012) Variability in the power-law distributions of rupture events. *Eur. Phys. J. Special Topics* **205**, 199-215. https://doi.org/10.1140/epjst/e2012-01571-9.

Amorese, D. (2007) Applying a change-point detection method on frequency-magnitude distributions. *Bull. Seismol. Soc. Am.* **97**, 1742-1749. https://doi.org/10.1785/0120060181

Ávila-Barrientos, L., Nava, F. (2020) Gutenberg-Richter *b* value studies along the Mexican subduction zone and data constraints. *Geofís. Int.* **59** (4), 285-298. *https://doi.org/10.22201/igeof.00167169p.2020.59.4.2019*

Burroughs, S., Tebbens, S. (2002) The upper-truncated power law applied to earthquake cumulative frequency-magnitude distributions: evidence for a time-independent scaling parameter. Bull. Seismol. Soc. Am. 92, 2983-2993 https://doi.org/10.1785/0120010191

DeSalvio, N., Rudolph, M. (2021) A Retrospective Analysis of b-Value Changes Preceding Strong Earthquakes. *Seismol. Res. Lett.*, *93*, 364–375. https://doi.org/10.1785/0220210149.

El-Isa, Z., Eaton, D. (2014) Spatiotemporal variations in the b-value of earthquake magnitude–frequency distributions: Classification and causes. *Tectonophysics,* **615**, 1-11. https://doi.org/10.1016/j.tecto.2013.12.001

Enescu, B., Ito, K. (2001) Some premonitory phenomena of the 1995 Hyogo-Ken Nanbu (Kobe) earthquake: seismicity, *b*-value and fractal dimension. Tectonophysics, 338(3-4), 297-314. https://doi.org/10.1016/S0040-1951(01)00085-3

Frohlich, C., Davis, S. (1993) Teleseismic *b* values; or, much ado about 1.0. *J. Geophys. Res.*, *98* (B1), 631–644. https://doi.org/10.1029/ 92JB01891

Fujii, Y., Matsu'ura, M. (2001) Regional difference in scaling laws for large earthquakes and its tectonic implication. Microscopic and Macroscopic Simulation: Towards Predictive Modelling of the Earthquake Process, 2283-2302.

Godano, C., Tramelli, A., Petrillo, G., & Convertito, V. (2024) Testing the predictive power of b value for Italian seismicity. *Seismica,* 3.1. https://doi.org/10.26443/seismica.v3i1.1084

Gutenberg, B., Richter,C. (1944) Frequency of earthquakes in California, *Bull Seism. Soc. Am.* **34**:185–188. https://doi.org/10.1785/BSSA0340040185

Guttorp (1987) On least-squares estimation of b values. Bull. Seism. Soc. Am. 77 (6): 2115–2124. https://doi.org/10.1785/BSSA0770062115

Hirata, T. (1989) A correlation between the b value and the fractal dimension of earthquakes. *Journal of Geophysical Research: Solid Earth, 94* (B6), 7507-7514. https://doi.org/10.1029/JB094iB06p07507

Hu, N., Han, P., Wang, R., Shi, F., Chen, L., Li, H. (2024) Spatial Heterogeneity of *b* Values in Northeastern Tibetan Plateau and Its Interpretation. *Entropy* **26**, 182. https://doi.org/10.3390/e26030182

Ishimoto, M. Iida, K. (1939) Observations sur les seisms enregistrés par le microseismograph construit dernièrement (I), *Bull. Earthquake Res. Inst. Univ. of Tokyo* **17**, 443-478.

Kijko, A. (2004) Estimation of the maximum magnitude earthquake mmax. *Pure. Appl. Geophys.* **161**, 1-27. https://doi.org/10.1007/s00024-004-2531-4

Li, Y., Chen, X. (2021) Variations in apparent stress and b value preceding the 2010 MW8.8 Bio-Bío, Chile earthquake. *Pure Appl. Geophys. 178*, 4797-4813 https://doi.org/10.1007/s00024-020-02637-3

Madariaga, R. (2010) *Earthquake scaling laws.* In Extreme Environmental Events: Complexity in Forecasting and Early Warning. RA Meyers ed., Springer, 364-382.

Main, I., Leonard, T., Papasouliotis, O., Hatton, C., Meredith, P. (1999) One slope or two? Detecting statistically significant breaks of slope in geophysical data, with application to fracture scaling relationships, Geophys. Res. Lett., 26(18), 2801–2804. https://doi.org/10.1029/1999GL005372

Main, I., O'Brien, G., Henderson, J. (2000) Statistical physics of earthquakes: Comparison of distribution exponents for source area and potential energy and the dynamic emergence of log-periodic energy quanta. Journal of Geophysical Research: Solid Earth, 105(B3), 6105-6126. https://doi.org/10.1029/1999JB900396

Main, I., Al-Kindy, F. (2002) Entropy, energy, and proximity to criticality in global earthquake populations, *Geophys. Res. Lett.* **29** (7). https://doi.org/10.1029/2001GL014078.

Mansinha, L., Shen, P. (1987) On the magnitude entropy of earthquakes. *Tectonophysics*, **138**(1), 115-119. https://doi.org/10.1016/0040-1951(87)90070-9

Marzocchi, W. & Sandri, L., 2003. A review and new insights on the estimation of the b-value and its uncertainty. *Ann Geophys*. 46(6), 1271–1282.

Nanjo, K., Hirata, N., Obara, K., Kasahara, K. (2012) Decade-scale decrease in *b* value prior to the M9-class 2011 Tohoku and 2004 Sumatra quakes. *Geophys. Res. Lett.* **39**, L20304. https://doi.org/10.1029/2012GL052997

Nava, F. (2024) Seismic magnitudes entropy and b-value. Acta Geophysica, 1-12. https://doi.org/10.1007/s11600-024-01424-1

Nuannin, P., Kulhanek, O., Persson, L. (2005) Spatial and temporal b value anomalies preceding the devastating off coast of NW Sumatra earthquake of December 26, 2004, Geophys. Res. Lett., 32, L11307. https://doi.org/10.1029/2005GL022679

Okal, E., Kirby, S. (1995) Frequency-moment distribution of deep earthquakes; implications for the seismogenic zone at the bottom of the slabs. *Physics of the Earth and Planetary Interiors* **92**, 169-187. https://doi.org/10.1016/0031-9201(95)03037-8

Olsson, R. (1999) An estimation of the maximum *b*-value in the Gutenberg-Richter relation. Geodynamics 27: 547-552. https://doi.org/10.1016/S0264-3707(98)00022-2

Oncel, A., Wilson, T., Nishizawa, O. (2001) Size scaling relationships in the active fault networks of Japan and their correlation with Gutenberg-Richter *b* values. *Journal of Geophysical Research* **106** (B10), 21,827-21,841. https://doi.org/10.1029/2000JB900408

Pacheco, J., Scholz, C., Sykes, L. (1992) Changes in frequency-size relationship from small to large earthquakes. *Nature* **335**, 71-73. https://doi.org/10.1038/355071a0

Pisarenko, V., Sornette, D. (2004) Statistical detection and characterization of a deviation from the Gutenberg–Richter distribution above magnitude 8. *Pure and Applied Geophysics* **161**, 839-864. https://doi.org/10.1007/s00024-003-2475-0

Richter, C. (1958) *Elementary seismology*. W.H.Freeman and Co., USA, 768pp.

Romanowicz, B., Rundle, J. (1993) On scaling relations for large earthquakes. *Bull. Seismol. Soc. Am.* **83**, 1294-1297. https://doi.org/10.1785/BSSA0830041294

Rundle, J. (1989) Derivation of the complete Gutenberg-Richter magnitude-frequency relation using the principle of scale invariance. Journal of Geophysical Research: Solid Earth, 94(B9), 12337-12342. https://doi.org/10.1029/JB094iB09p12337

Rundle, J., Turcotte, D., Shcherbakov, R., Klein, W., Sammis, C. (2003) Statistical physics approach to understanding the multiscale dynamics of earthquake fault systems. Reviews of Geophysics, 41(4). https://doi.org/10.1029/2003RG000135

Scholz, C. (1982) Scaling laws for large earthquakes: consequences for physical models. Bull. Seismol. Soc. Am. 72, 1-14. https://doi.org/10.1785/BSSA0720010001

Scholz, C. (1997) Size distributions for large and small earthquakes. *Bull. Seismol. Soc. Am.* **87**, 1074-1077. https://doi.org/10.1785/BSSA0870041074

Scholtz, C. (2015) On the stress dependence of the earthquake *b* value. *Geophys. Res. Lett.* **42**, 1399-1402. https://doi.org/10.1002/2014GL062863

Schorlemmer, D., Wiemer, S., Wyss, M. (2005) Variations in earthquake-size distribution across different stress regimes, *Nature* **437**, 539–542. https://doi.org/10.1038/nature04094

Singh, S., Rodriguez, M., Esteva, L. (1983) Statistics of small earthquakes and frequency of occurrence of large earthquakes along the Mexican subduction zone. *Bull. Seismol. Soc. Am.* **73**, 1779-1796. https://doi.org/10.1785/BSSA07306A1779

Singh C, Singh A, Chadha R (2009) Fractal and b-Value Mapping in Eastern Himalaya and Southern Tibet. *Bull Seismol Soc Am* **99**, 3529–3533. https://doi.org/10.1785/0120090041

Sornette, D., Knopoff, L., Kagan, Y., Vanneste, C. (1996) Rank-ordering statistics of extreme events: application to the distribution of large events. J. Geophys. Res. 101, 13883–13893. https://doi.org/10.1029/96JB00177

Sornette, D., Sornette, A. (1999) General theory of the modified Gutenberg-Richter law for large seismic moments. Bull. Seismo. Soc. Am. 89: 1121-1130. https://doi.org/10.1785/BSSA0890041121

Tinti S. & Mulargia, F., 1987. Confidence intervals of b-values for grouped magnitudes. Bull. Seismo. Soc. Am. 77, 2125–2134. https://doi.org/10.1785/BSSA0770062125

Triep, E., Sykes, L. (1997) Frequency of occurrence of moderate to great earthquakes in intracontinental regions: Implications for changes in stress, earthquake prediction, and hazards assessment. J. *Geophys Res.* **102** (B5), 9923-9948. https://doi.org/10.1029/96JB03900

Utsu, T. (1965) A method for determining the value of b in a formula log n = a - bM showing the magnitude-frequency relation for earthquakes. *Geophys Bull Hokkaido Univ* **13**: 99–103.

Utsu, T. (2002). Statistical features of seismicity. In *International Handbook of Earthquake & Engineering Seismology*, Lee, W., Kanamori, H., Jennings, P., Kisslinger, C. (Eds.), 43, 719-732.

Wang, J. (2016) A mechanism causing *b*-value anomalies prior to a mainshock. *Bull. Seismo. Soc. Am., 106,* 1663-1671. https://doi.org/10.1785/0120150335

Wiemer, S., McNutt, S. (1997) Variations in the frequency-magnitude distribution with depth in two volcanic areas: Mount St. Helens, Washington, and Mt. Spurr, Alaska. Geophysical Research Letters 24(2): 189-192. https://doi.org/10.1029/96GL03779

Wiemer, S., Wyss, M. (2002) Mapping spatial variability of the frequency-magnitude distribution of earthquakes. Adv Geophys 45, 259–302. https://doi.org/10.1016/S0065-2687(02)80007-3

Wyss, M. (1973) Towards a Physical Understanding of the Earthquake Frequency Distribution. *Geophysical Journal of the Royal Astronomical Society*, *31*(4):341–359. https://doi.org/10.1111/j.1365- 246X.1973.tb06506.x

Wyss, M., Shimazaki, K., Wiemer, S. (1997) Mapping active magma chambers by b-value beneath the off-Ito volcano, Japan. J. Geophys. Res. 102, 20413-20422. https://doi.org/10.1029/97JB01074

Wyss, M., Sammis, C., Nadeau, R., Wiemer, S. (2004) Fractal dimension and b-value on creeping and locked patches of the San Andreas fault near Parkfield, California. *Bull. Seismo. Soc. Am., 94* (2), 410–421. https://doi.org/10.1785/0120030054

Zhan, Z. (2017) Gutenberg-Richter law for deep earthquakes revisited: A dual mechanism hypothesis. Earth and Planetary Science Letters 461, 1-7. https://doi.org/10.1016/j.epsl.2016.12.030